Avestia Publishing
Journal Name: Journal of Fluid Flow, Heat and Mass Transfer (JFFHMT)
Volume 12, Year 2025
ISSN: 2368-6111
DOI: 10.11159/jffhmt.2025.035

Heat Transfer Enhancement through Thermal Dispersion in Hybrid Nanofluid Saturated Mixed Convection along a Horizontal Cone

Nayema Islam Nima[1], Shahina Akter[2] , Jahangir Alam[3]
[1]Department of Physical Sciences, Independent University, Bangladesh (IUB), Dhaka 1229, Bangladesh; nayema@iub.edu.bd.
[2]Department of Quantitative Sciences, International University of Business Agriculture and Technology, Dhaka 1230, Bangladesh; shahina.qs@iubat.edu.
[3]Department of Computer Science and Mathematics, Bangladesh Agricultural University, Mymensingh-2202, Bangladesh. jahangiralam.csm@bau.edu.bd.

Abstract- This study explores the influence of thermal dispersion on mixed convection flow of a hybrid nanofluid past a horizontal cone. The working fluid is ethylene glycol containing cylindrical alumina (Al_2O_3) and silica (SiO_2) nanoparticles in equal volume fractions. Compared with a single alumina-based nanofluid, the hybrid suspension exhibits significantly improved thermal transport capability. To analyze the problem, the governing nonlinear partial differential equations are reduced to ordinary differential equations using similarity transformations, and the resulting system is solved numerically with the Bvp4c method. The investigation shows that suction strongly enhances the heat transfer rate by reducing the thickness of the thermal boundary layer, while injection diminishes it, particularly under forced convection conditions. Thermal dispersion is found to decrease heat transfer efficiency by weakening the near-wall temperature gradient, with its impact being more pronounced in forced and mixed convection regions. In contrast, a higher Biot number consistently increases heat transfer, with stronger effects observed as the flow approaches free convection dominance. Overall, the results demonstrate that hybrid nanofluids, when coupled with optimized boundary conditions, can deliver substantial improvements in convective heat transfer performance. These findings underscore the potential application of such fluids in advanced cooling systems, heat exchangers, and energy-related technologies where efficient thermal regulation is critical.

Keywords: dispersion, suction/injection, hybrid nanofluid, ethylene glycol, forced convection.

Nomenclature

a^*	Co-efficient of thermal dispersion
B_{iot}	Biot number of heat transfer
g	Acceleration due to gravity
k	Permeability parameter
Ra_x	Local Rayleigh number
Pe_x	Local peclet number
Pe_d	Pore dependent peclet number
s^*	Suction/injection parameter
T	Temperature
T_f	Wall temperature
T_∞	Ambient temperature
u^*, v^*	Velocity components along x^* & y^* axes
x^*, y^*	Cartesian coordinates

Greek symbols

α_e^*	Effective thermal diffusivity
ρ	Fluid density
λ_m	Mixed convection parameter
η	Similarity parameter
ϖ	Angle
ψ	Stream function

Date Received: 2025-06-01
Date Revised: 2025-09-17
Date Accepted: 2025-10-01
Date Published: 2025-11-26

1. Introduction

Mixed convection arises when buoyancy and forced flow act together. It is a critical mechanism in compact thermal systems such as electronics cooling, solar collectors, and heat exchangers. By influencing boundary-layer behavior across Reynolds–Grashof ranges, mixed convection directly shapes thermal performance. Previous studies have shown that geometry and orientation strongly affect flow structures and heat transfer. This makes mixed convection especially important in porous and non-planar domains (Amran et al. [1]). Recent experimental and numerical research confirms that nanofluids and hybrid nanofluids can enhance heat transfer in forced and mixed convection regimes. Compared with base fluids, they increase Nusselt numbers and thin thermal boundary layers (Roy & Akter [2]; Ali et al. [3]; Atofarati et al. [5]). These results reinforce the link between convection regimes and nanoparticle-enhanced transport.

Nanofluids, which are suspensions of nanoparticles in conventional base fluids, have attracted wide attention in thermal sciences. They improve thermal conductivity, adjust viscosity, and strengthen convective heat transfer (Choi [5]). Building on this concept, hybrid nanofluids combine two or more different nanoparticles. Such mixtures provide synergistic improvements in thermal transport compared to mono nanofluids (Sarkar et al. [6]; Sundar et al. [7]). Many studies have confirmed their enhanced stability and heat transfer behavior across various applications. For example, Shaik et al. [8] demonstrated the superior thermophysical properties of Cu–Graphene/water hybrid nanofluids. Sarfraz et al. [9] compared thermal conductivity models and showed consistent improvements with hybrid suspensions. Shahid et al. [10] highlighted the role of mixed convection in cavity flows with hybrid nanofluids. Asghar et al. [11] extended this analysis by incorporating magnetic field and heat generation effects (Ibrahim et al. [12]; Theeb et al. [13]).

Despite these advances, the influence of thermal dispersion has not been widely examined. Thermal dispersion results from microscopic conduction and particle-induced mixing, and it can strongly alter heat transport in porous systems. For instance, Wahid et al. [14] studied radiative mixed convection of hybrid nanofluids near a vertical flat plate and reported the sensitivity of heat transfer to Soret and Dufour effects mechanisms related to dispersion. Riaz et al. [15] investigated hybrid nanofluids in cylindrical systems and emphasized geometry-driven variations in flow and temperature. Rashid et al. [16] analyzed suction and magnetic effects over stretching surfaces, highlighting the importance of boundary conditions. More recently, Wahid et al. [17] and Mahdy et al. [18] modeled mixed convection in porous media and demonstrated that permeability and dispersion strongly influence forced–natural convection interactions. However, none of these works directly studied thermal dispersion in hybrid nanofluid flow over a horizontal cone.

Hybrid nanofluids have been widely examined in mixed convection flows (Roy & Akter [2]; Shahid et al. [10]; Asghar et al. [11]). Yet most studies focused on nanoparticle composition, radiation, magnetic fields, or suction effects, usually in flat or stretching surface configurations. The explicit role of thermal dispersion has been largely overlooked. Wahid et al. [14] and Riaz et al. [15] examined related transport mechanisms, but did not address hybrid suspensions in detail. Mahdy et al. [18] and Wahid et al. [17] explored porous domains, but concentrated on permeability and magnetic influences rather than dispersion itself.

This gap is significant because dispersion modifies temperature gradients and reshapes heat transport characteristics. To address it, the present work investigates the combined effects of thermal dispersion, suction/injection, and Biot number on hybrid nanofluid flow over a horizontal cone. The working fluid is an Al_2O_3–SiO_2/ethylene glycol hybrid suspension. To the best of our knowledge, this is the first comprehensive study that incorporates thermal dispersion into the analysis of hybrid nanofluid mixed convection over a horizontal cone. The findings provide new insights for designing efficient thermal management and energy systems.

2. Mathematical modelling

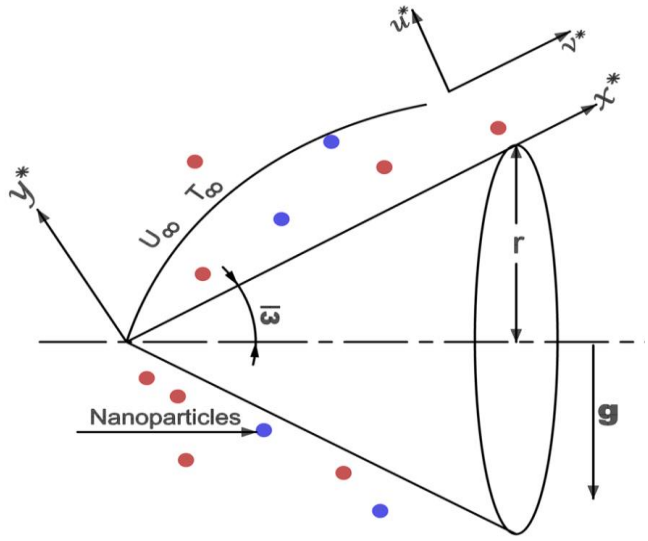

Figure 1. The coordinate geometry

This study considers a steady, laminar, mixed convection boundary layer flow over a semi-vertically inclined horizontal cone embedded within a porous medium saturated by fluid, where the ambient temperature is denoted by T_∞. The cone surface is subjected to convective heating from a warm hybrid nanofluid maintained at a uniform temperature T_f, with a spatially varying heat transfer coefficient $h_f(x^*)$ along the surface. The coordinate system for the flow configuration is illustrated in Figure 1. The x^* axis is taken along the surface of the semi-vertically inclined horizontal cone, measured from the cone vertex, while the y^* axis is oriented normal to the surface into the fluid. Employing the Boussinesq approximation, the governing conservation equations namely, the continuity, momentum and energy equations as Ferdows et al. [19], Sarfraz et al. [20] are formulated, incorporating thermal dispersion effects and a convective boundary condition at the surface.

$$\frac{\partial(ru^*)}{\partial x^*}+\frac{\partial(rv^*)}{\partial y^*}=0 \tag{1}$$

$$\frac{\partial u^*}{\partial y^*}=-\frac{\partial}{\partial x^*}\left(\frac{gk(\rho\beta)_{hbnf}}{\mu_{hbnf}}(T-T_\infty)\cos\varpi\right) \tag{2}$$

$$u^*\frac{\partial T}{\partial x^*}+v^*\frac{\partial T}{\partial y^*}=\frac{\partial}{\partial y^*}\left(\alpha^*_e\frac{\partial T}{\partial y^*}\right) \tag{3}$$

Boundary conditions

$$v^*=v^*_w,-k_{hbnf}\frac{\partial T}{\partial y}=h_f(x^*)(T_f-T)\text{ at }y=0$$
$$u^*\to u_\infty{}^*,T\to T_\infty\text{ at }y\to\infty \tag{4}$$

Where $\alpha^*_e=\alpha_{hbnf}+a^*du=\dfrac{k_{hbnf}}{(\rho_{cp})_{hbnf}}+a^*du$ (5)

Here $\alpha^*_e,\alpha_{hbnf},a^*$ are effective thermal, constant thermal and coefficient of thermal dispersion respectively. a^* value is between $\frac{1}{7}$ to $\frac{1}{3}$.

Transformations

$$\eta=\left(\frac{u^*_\infty}{\alpha_f x^*}\right)^{0.5}y,\psi=(\alpha_f u^*_\infty)^{0.5}r^*f(\eta),\theta(\eta)=\frac{T-T_\infty}{T_f-T_\infty} \tag{6}$$

Using (5) and (6), transformed equations (1-4) are as follows:

$$f''=\frac{\dfrac{(\rho\beta)_{hbnf}}{(\rho\beta)_f}}{\dfrac{\mu_{hbnf}}{\mu_f}}\lambda_m{}^3\frac{\eta}{2}\theta' \tag{7}$$

$$\frac{\dfrac{k_{hbnf}}{k_f}}{\dfrac{(\rho_{cp})_{hbnf}}{(\rho_{cp})_f}}\theta''+\frac{1}{2}f\theta'+a^*Pe_d(f'\theta''+f''\theta')=0 \tag{8}$$

Boundary Conditions

$$f=s^*,\frac{k_{hbnf}}{k_f}\theta'=-B_{iot}(1-\theta(0))\quad\text{at }\eta=0$$
$$f'=1,\theta\to0\quad\text{at }\eta\to\infty \tag{9}$$

Mononanofluid and Hybrid nanofluid properties are shown in Table 1. and Table 2. Different physical

parameter can be defined are as follows: $\lambda_m = \frac{Ra_x^{\frac{1}{3}}}{Pe_x^{\frac{1}{2}}}$,

$$Ra_x = \frac{gk(\rho\beta)_f (T_f - T_\infty)x^* \cos\varpi}{\mu_f \alpha_f}, Pe_x = \frac{u_\infty^* x^*}{\alpha_f},$$

$$B_{iot} = \frac{-h_f \alpha_f^{0.5}}{k_f u_\infty^{0.5}}, h_f(x^*) = x^{-0.5} h_f$$

Table 1. Nanofluid properties

$\rho_{nf} = ((1-\phi_1)\rho_f + \phi_1 \rho_{Al_2o_3})$ $(\rho_{c_p})_{nf} = ((1-\phi_1)(\rho_{c_p})_f + \phi_1 (\rho_{c_p})_{Al_2o_3})$ $(\rho_\beta)_{nf} = ((1-\phi_1)(\rho_\beta)_f + \phi_1 (\rho_\beta)_{Al_2o_3})$ $\frac{k_{nf}}{k_f} = \frac{k_{Al_2o_3} + (r_1-1)k_f - (r_2-1)(k_f - k_{Al_2o_3})\phi_1}{k_{Al_2o_3} + (r_1-1)k_f + (k_f - k_{Al_2o_3})\phi_1}$ $\mu_{nf} = \frac{\mu_f}{(1-\phi_1)^{2.5}}, \upsilon_{nf} = \frac{\mu_{nf}}{\rho_{nf}}$
$\rho_{hbnf} = (1-\phi_2)((1-\phi_1)\rho_f + \phi_1 \rho_{Al_2o_3}) + \phi_2 \rho_{sio_2}$ $(\rho_{c_p})_{hbnf} = (1-\phi_2)((1-\phi_1)(\rho_{c_p})_f + \phi_1 (\rho_{c_p})_{Al_2o_3}) + \phi_2 (\rho_{c_p})_{sio_2}$ $(\rho_\beta)_{hbnf} = (1-\phi_2)((1-\phi_1)(\rho_\beta)_f + \phi_1 (\rho_\beta)_{Al_2o_3}) + \phi_2 (\rho_\beta)_{sio_2}$ $\frac{k_{hbnf}}{k_f} = \frac{k_{sio_2} + (r_1-1)k_{b_f} - (r_1-1)(k_{bf} - k_{sio_2})\phi_2}{k_{sio_2} + (r_1-1)k_{b_f} + (k_{bf} - k_{sio_2})\phi_2},$ $\frac{k_{bf}}{k_f} = \frac{k_{Al_2o_3} + (r_1-1)k_f - (r_1-1)(k_f - k_{Al_2o_3})\phi_1}{k_{Al_2o_3} + (r_1-1)k_f + (k_f - k_{Al_2o_3})\phi_1}$ $\mu_{hbnf} = \frac{\mu_f}{(1-\phi_1)^{2.5}(1-\phi_2)^{2.5}}, \upsilon_{hbnf} = \frac{\mu_{hbnf}}{\rho_{hbnf}}$

According to Sarfraz et al. [12], the shape factor for the nanoparticles $r_1 = 6$ is selected in the aforementioned expressions, as our study focuses on cylindrical-shaped nanoparticles.

Table 2. Physical properties of nanoparticles and basefluid

Physical Properties	Nanoparticles		Base Fluid
	Alumina	Silica	Ethylene glycole
c_p	765	745	2430
k	46	1.38	0.253
β	0.85×10^{-6}	0.55×10^{-6}	0.57×10^{-6}
ρ	3970	2220	1115

$$P_1 = \frac{\mu_{hbnf}}{\mu_f}, P_2 = \frac{(\rho_\beta)_{hbnf}}{(\rho_\beta)_f}, P_3 = \frac{(\rho_{c_p})_{hbnf}}{(\rho_{c_p})_f}, P_4 = \frac{k_{hbnf}}{k_f} \quad (10)$$

3. Numerical solution

The nonlinear ordinary differential equations, derived from the governing partial differential equations via similarity transformations, are solved numerically using MATLAB's **bvp4c** solver. This approach, well-suited for two-point boundary value problems, reformulates the higher-order system into first-order equations, defined alongside boundary conditions through function handles. An initial guess, guided by physical considerations, is supplied to initiate the computation. The **bvp4c** algorithm employs a collocation method with adaptive mesh refinement, ensuring convergence by iteratively minimizing residual errors until the prescribed tolerance is satisfied.

Now substituting η for x^* and also considering

$$h_1 = f, h_2 = f', h_3 = \theta, h_4 = \theta'$$

The first order equations are

$$\frac{dh_1}{dx} = f' = h_2,$$

$$\frac{dh_2}{dx} = f'' = \frac{p_2}{p_1} * \lambda^3 * \frac{\eta}{2} * h_4$$

$$\frac{dh_3}{dx} = \theta' = h_4,$$

$$\frac{dh_4}{dx} = \theta'' = (-0.5 * h_1 * h_4 - a * Pe_d *$$

$$(\frac{p_2}{p_1} * \lambda^3 * \frac{\eta}{2} * h_4)) / (\frac{p_4}{p_3} + a^* * Pe_d * h_2)$$

Boundary conditions

$$hp(1) - s^* = 0, \qquad hq(2) - 1 = 0$$

$$p_4 * hp(4) + B_{iot} * (1 - hp(3)) = 0, \; hq(3) = 0$$

The variable hp represents the boundary condition on the left side, while hq denotes the boundary condition on the right. To assess the accuracy of the present numerical solutions, a comparison was

carried out with the results reported by Ferdows et al. [19] for a particular case, as summarized in Table 3 and Table 4. The close agreement between both sets of results verifies the robustness and accuracy of the proposed computational method.

Table 3. Biot number B_{iot} and Dispersion effect on $f'(0)$ for the regular fluid ($\phi_1 = \phi_2 = 0$)

B_{iot}	Pe_d	$f'(0)$	
		Present study	Ferdows et al. [19]
10000000	0	1.0000	1.0000
1.5	0	1.0000	1.0000
1.5	10	1.0000	1.0000

Table 4. Biot number B_{iot} and Dispersion effect on $-\theta'(0)$ for the regular fluid ($\phi_1 = \phi_2 = 0$)

B_{iot}	Pe_d	$-\theta'(0)$	
		Present study	Ferdows et al. [19]
10000000	0	0.5644	0.5644
1.5	0	0.4101	0.4100
1.5	10	0.2539	0.2538

4. Results discussion

In this analysis, the nanofluid contains 4% volume fraction of alumina nanoparticles ($\phi_1 = 0.04, \phi_2 = 0.00$), whereas the hybrid nanofluid consists of 2% alumina and 2% silica nanoparticles ($\phi_1 = 0.02, \phi_2 = 0.02$). The values of $f'(0)$ are tabulated in Table 5 to illustrate the effect of the mixed convection parameter on the velocity profile at the surface. Here, λ_m corresponds to pure forced convection, and increasing λ_m shifts the flow from forced to mixed and eventually toward free convection. The table presents the impact of λ_m for the mono nanofluid, hybrid nanofluid, and the regular base fluid for comparison.

Table 5. Mixed convection effect on $f'(0)$ for the the values $B_{iot} = 1.5, Pe_d = 1, a^* = 0.3, s^* = 0$

λ_m	$f'(0)$		
	$\phi_1 = 0.04,$ $\phi_2 = 0.00$	$\phi_1 = 0.02,$ $\phi_2 = 0.02$	$\phi_1 = 0.00,$ $\phi_2 = 0.00$
0	1.00000	1.00000	1.00000
0.2	1.00408	1.00390	1.00386
0.4	1.03234	1.03094	1.03063
0.6	1.10655	1.10201	1.10106
1.0	1.44928	1.43059	1.42754
2.0	3.66174	3.54279	3.54274

The table illustrates how the dimensionless wall shear, $f'(0)$ varies with λ_m, the mixed convection parameter. Regular fluid, mono nanofluid, and hybrid nanofluid exhibit the similar behaviour at surface as buoyancy effects are negligible. As λ_m increases, indicating a shift toward mixed and free convection, $f'(0)$ rises for all fluids due to enhanced wall shear from buoyancy-driven momentum transport. The mono nanofluid shows slightly higher $f'(0)$ at lower λ_m. At higher λ_m, the hybrid nanofluid surpasses it. This reflects the synergistic effect of the two nanoparticle types in enhancing convective momentum transfer. The regular fluid consistently exhibits the lowest λ_m, highlighting the significant role of nanoparticles in increasing skin friction. Overall, the table demonstrates that mixed convection strengthens wall shear and that hybrid nanofluids provide superior momentum transport compared to mono nanofluids under identical flow conditions.

Figure 2 demonstrates the influence of suction and injection on the velocity profile of the boundary layer flow. Suction, which extracts fluid from the surface, reduces the boundary layer thickness and sharpens the velocity gradient near the wall, thereby stabilizing the flow. In contrast, injection introduces additional fluid into the boundary layer, which increases its thickness and leads to a relatively flatter velocity distribution. When comparing different fluids, the hybrid nanofluid consistently exhibits a thinner boundary layer and a steeper velocity gradient compared to the mono nanofluid. This behavior is attributed to the synergistic effect of alumina and silica nanoparticles, which enhances both momentum and thermal diffusivities, thereby intensifying velocity near the wall region.

Figure 3 highlights the role of thermal dispersion on the velocity distribution. As the dispersion parameter increases, the velocity profile rises near the surface, indicating that enhanced thermal dispersion promotes a more efficient distribution of thermal energy within the fluid, which in turn accelerates fluid motion close to the wall. The effect is more pronounced in hybrid nanofluids, as the combined nanoparticles facilitate stronger thermal conductivity and convective interactions than mono nanofluids.

Overall, Figures 2 and 3 show that hybrid nanofluids outperform mono nanofluids in boundary layer control and flow enhancement. This improvement occurs under the combined effects of suction, injection, and thermal dispersion. This indicates their superior potential in applications requiring efficient thermal management and convective heat transfer augmentation.

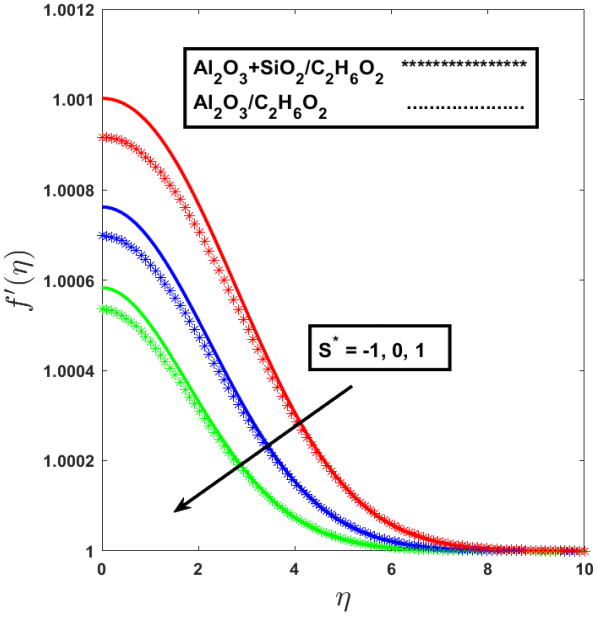

Figure 2. Mono nanofluid / hybrid nanofluid impact on velocity profile with suction/injection effect

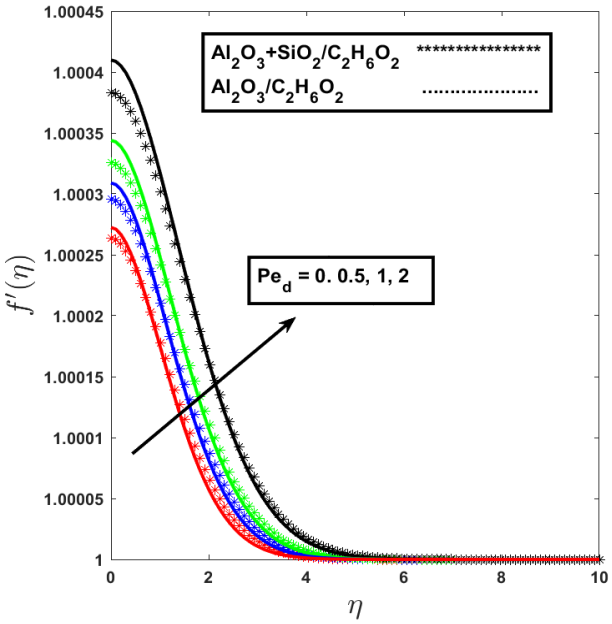

Figure 3. Mono nanofluid / hybrid nanofluid impact on velocity profile with dispersion effect.

Figure 4 illustrates the effect of the Biot number on the surface heat transfer rate for varying values of the mixed convection parameter λ_m. When $\lambda_m = 0$, the flow corresponds to pure forced convection, while increasing values of λ_m reflect a transition toward mixed and ultimately free convection, where buoyancy effects dominate. As the Biot number increases from 0.5 to 1.5, the heat transfer rate (represented through the Nusselt number) rises steadily. This enhancement is attributed to the stronger convective heat exchange at the fluid–solid interface, since a higher Biot number signifies more efficient energy transfer from the surface into the fluid medium.

Across all values of λ_m, the hybrid nanofluid demonstrates a consistently higher heat transfer rate compared to the mono nanofluid and the base fluid. This superior performance results from the synergistic thermal properties of alumina and silica nanoparticles. They collectively improve thermal conductivity, enhance energy transport mechanisms, and reduce thermal boundary layer thickness. The improvement becomes especially prominent under stronger buoyancy-driven conditions (higher λ_m). Here, the interplay between thermal dispersion and convection further augments the heat transfer. This establishes their suitability for thermal systems where both conduction and convection mechanisms are critical.

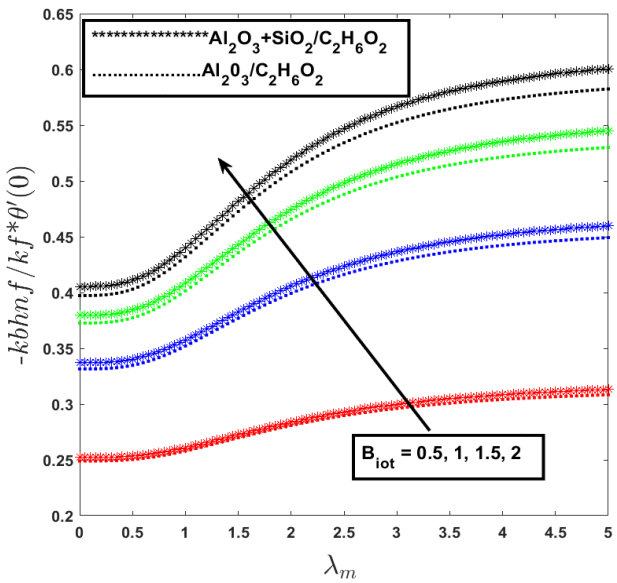

Figure 4. Effect of mono nanofluid and hybrid nanofluid on heat transfer rate with the variation of biot number

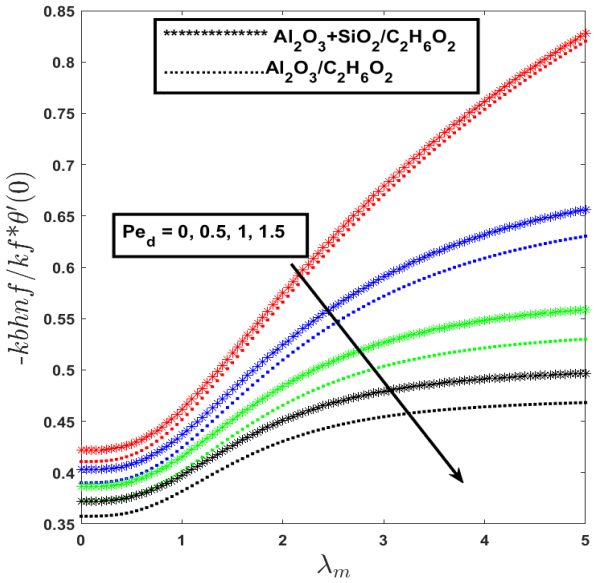

Figure 5. Effect of mono nanofluid and hybrid nanofluid on heat transfer rate with the variation of dispersion parameter

Figure 5 shows that lower thermal dispersion corresponds to higher heat transfer rates, as it maintains a steeper surface temperature gradient. In contrast, stronger dispersion redistributes thermal energy within the fluid, smoothing the temperature profile and weakening heat transfer. When the mixed convection parameter (λ_m) lies between 0 and 1, corresponding to the transition from forced to mixed convection, the heat transfer rate remains relatively modest. However, as λ_m exceeds 1, entering the free convection–dominated regime, the heat transfer rate increases significantly. This enhancement is most pronounced for the hybrid nanofluid. It underscores its greater sensitivity to buoyancy-driven mechanisms and its superior thermal transport capability compared to the mono nanofluid.

Figure 6 highlights the influence of the suction/injection parameter s^*. Suction $s^* > 0$ enhances heat transfer by reducing the thermal boundary layer thickness, while injection $s^* < 0$ weakens heat transfer by supplying additional fluid at the surface. The no mass transfer case $s^* = 0$ shows only a minor decrease. These effects are strongest in the forced convection region $\lambda_m = 0$, diminish progressively in the mixed convection regime, and become negligible when buoyancy $\lambda_m > 1$. The hybrid nanofluid consistently benefits more from suction. It reflects its enhanced momentum and thermal diffusivity due to the combined effects of alumina and silica nanoparticles.

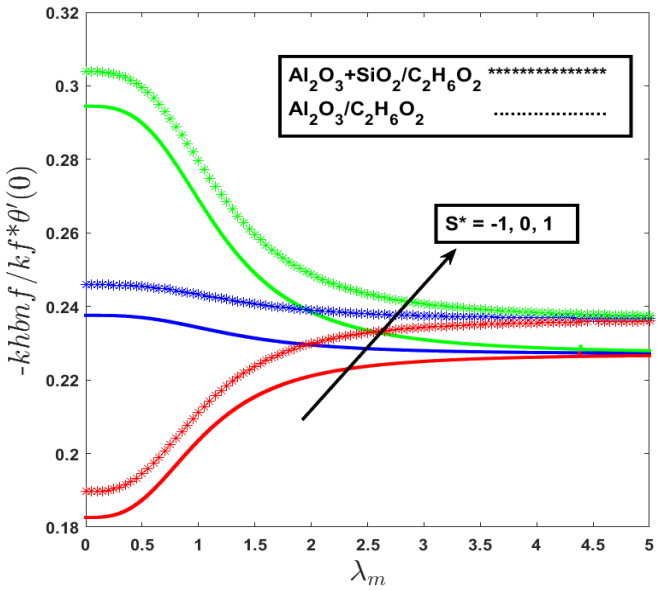

Figure 6. Effect of mono nanofluid and hybrid nanofluid on heat transfer rate with the variation of suction/injection parameter

So, thermal dispersion and suction/injection strongly influence heat transfer behavior in the forced and mixed convection regimes, while in free convection conditions, buoyancy effects dominate. The hybrid nanofluid demonstrates superior adaptability and higher thermal performance across all regimes.

To further illustrate the significance of thermal dispersion in hybrid nanofluid transport, **Table 6** presents the variation of surface temperature distribution $\theta(0)$ with respect to the pore dependent Peclet number Pe_d. The data include results for the mono nanofluid, hybrid nanofluid, and the regular base fluid. The data clearly indicate that $\theta(0)$ increases monotonically with Pe_d, reflecting stronger dispersion-induced thermal mixing. Among the three cases, the hybrid nanofluid consistently shows slightly lower surface temperature values than the mono nanofluid and base fluid. This implies more efficient heat removal due to the combined nanoparticle effect. The differences become more pronounced at higher Peclet numbers, emphasizing the hybrid suspension's superior capacity to manage heat transport under enhanced dispersion conditions. This behavior highlights the necessity of incorporating dispersion effects in analyzing mixed convection of hybrid nanofluids over different porous geometries. This aspect is the central focus of the present work.

Table 6. Dispersion effect on $\theta(0)$ for the the values $B_{iot}=1.5, \lambda_m=0.5, a^*=0.3, s^*=0$

Pe_d	$\theta(0)$		
	$\phi_1=0.04,$ $\phi_2=0.00$	$\phi_1=0.02,$ $\phi_2=0.02$	$\phi_1=0.00,$ $\phi_2=0.00$
0	0.72192	0.71843	0.72262
0.5	0.73626	0.73213	0.73685
1.0	0.74844	0.74387	0.74894
2.0	0.76818	0.76308	0.76856
5.0	0.80683	0.80127	0.80702
10	0.84198	0.83658	0.84204

5. Conclusion

This work presented a numerical investigation of hybrid nanofluid mixed convection over a horizontal cone with the inclusion of thermal dispersion effects. Alumina–silica nanoparticles suspended in ethylene glycol were considered, and the governing equations were solved through similarity transformations and the Bvp4c method. The analysis establishes that hybrid nanofluids provide distinct thermal and flow advantages compared to mono nanofluids and the pure base fluid. The combined presence of multiple nanoparticles improved transport efficiency in porous geometries, offering performance benefits relevant to engineering systems. Key controlling parameters, such as the Biot number, dispersion strength, and suction/injection conditions, were shown to strongly influence system response, underscoring the complexity of heat and momentum transfer in such configurations.

Overall, the outcomes emphasize the relevance of hybrid nanofluids in enhancing convection-driven energy transport for practical applications in energy harvesting, cooling technologies, and compact heat exchangers.

5.1. Future Work

Building on this study, future research can address temperature-dependent thermophysical properties and extend the model to non-Newtonian hybrid nanofluids. External influences such as magnetic or electric fields, thermal radiation, or chemical reactions could also be incorporated to capture more realistic operating conditions. Entropy generation and second-law analyses may provide deeper insights into system efficiency. Furthermore, experimental validation

of the theoretical findings would be essential to translate these results into practical design strategies for advanced thermal management technologies.

Acknowledgement

The authors gratefully acknowledge the support received from the VC's Research Fund 2024 (VCRF-SETS:24-029), Independent University, Bangladesh (IUB), during the course of this work.

References

[1] M. F. Amran, N. M. Anas, and M. Z. Abdullah, "Effects of Prandtl number, geometry, and orientation on mixed convection heat transfer: A review," *Processes*, vol. 12, no. 12, p. 2749, 2024. https://doi.org/10.3390/pr12122749

[2] N. C. Roy and A. Akter, "Dual solutions of mixed convective hybrid nanofluid flow over a shrinking cylinder placed in a porous medium," *Heliyon*, vol. 9, no. 11, e22166, 2023. https://doi.org/10.1016/j.heliyon.2023.e22166

[3] S. A. Ali, M. R. Hameed, and H. K. Kadhim, "Effect of Al_2O_3/H_2O Nanofluid on the Flow and Forced Convection Heat Transfer Enhancement in a Pipe Using Commercial CFD Code," *Iraqi J. Indust. Res.*, vol. 11, no. 3, pp. 11–24, 2024. https://doi.org/10.53523/ijoirVol11I3ID474

[4] E. O. Atofarati, A. O. Oyedeko, and S. A. Afolabi, "Nanofluids for heat transfer enhancement: a comprehensive review," *Cogent Engineering*, vol. 11, no. 1, p. 2434623, 2024. https://doi.org/10.1080/23311916.2024.2434623

[5] S. U. Choi and J. A. Eastman, "Enhancing thermal conductivity of fluids with nanoparticles," ANL/MSD/CP-84938; CONF-951135-29, Argonne National Lab., Argonne, IL, USA, 1995.

[6] J. Sarkar, P. Ghosh, and A. Adil, "A review on hybrid nanofluids: Recent research, development and applications," *Renewable and Sustainable Energy Reviews*, vol. 43, pp. 164–177, 2015. https://doi.org/10.1016/j.rser.2014.11.023

[7] L. S. Sundar, M. K. Singh, and A. C. M. Sousa, "Investigation of thermal conductivity and viscosity of Fe_3O_4 nanofluid for heat transfer applications," *International Communications in Heat and Mass Transfer*, vol. 44, pp. 7–14, 2013. 10.1016/j.icheatmasstransfer.2013.02.014

[8] A.H. Shaik, S. Chakraborty, S. Saboor, K.R. Kumar, A. Majumdar, M. Rizwan, M. Arıcı, and M.R. Chandan, "Cu-Graphene water-based hybrid nanofluids: synthesis, stability, thermophysical characterization, and figure of merit analysis," *J. Therm. Anal. Calorim.*, vol. 149, pp. 2953–2968, 2024. https://doi.org/10.1007/s10973-023-12875-x

[9] M. Sarfraz, M. Yasir, and M. Khan, "Exploring dual solutions and thermal conductivity in hybrid nanofluids: a comparative study of Xue and Hamilton–Crosser models," *Nanoscale Adv.*, vol. 5, pp. 6695–6704, 2023. 10.1039/D3NA00503H

[10] M. A. Shahid, M. Dayer, , I. Hashim, A. I. Alsabery & S. Momani, "Numerical investigation of multiphase flow effects on mixed convection in partially heated hybrid nanofluid-filled cavity," *J. Therm. Anal. Calorim.*, 2024. https://doi.org/10.1007/s10973-023-12860-4.

[11] A. Asghar, A. F. Chandio, Z. Shah, N. Vrinceanu, W. Deebani, M. Shutaywi, & L. A. Lund, "Magnetized mixed convection hybrid nanofluid with effect of heat generation/absorption and velocity slip condition," *Heliyon*, vol. 9, no. 2, e13189,2023. 10.1016/j.heliyon.2023.e13189

[12] I. U. Ibrahim, M. H. Khan, and A. Raza, "Mixed convection heat transfer characteristics of Al_2O_3–MWCNT hybrid nanofluid under thermally developing flow: Effects of particle percentage weight composition," *Appl. Therm. Eng.*, vol. 249, p. 123372, 2024. https://doi.org/10.1016/j.applthermaleng.2024.123372

[13] M. A. Theeb, A. Abdulkadhim, N. H. Hamza, M. F. Al-Dawody, M. Sheremet, and W. J. Kadhem, "Hybrid nanofluid mixed convection in a lid-driven wavy cavity with internal heated plate," *Results in Surfaces and Interfaces*, vol. 18, p. 100469, 2025. https://doi.org/10.1016/j.rsurfi.2025.100469

[14] N. S. Wahid, N. M. Arifin, N. S. Khashi'ie, I. Pop, N. Bachok, & M. E. H. Hafidzuddin, "Hybrid nanofluid radiative mixed convection stagnation point flow past a vertical flat plate with Dufour and Soret effects,"*Mathematics*, vol. 10, no. 16, p. 2966, 2022. https://doi.org/10.3390/math10162966

[15] A. Riaz, A. Abbasi, K. Al-Khaled, S.U. Khan, W. Farooq, E.S.M.T. El-Din , "A numerical analysis of the transport of modified hybrid nanofluids containing various nanoparticles with mixed convection applications in a vertical cylinder," *Front. Phys.*, vol. 10, 1018148, 2022. https://doi.org/10.3389/fphy.2022.1018148

[16] A. Rashid, M. Ayaz, and S. Islam, "Numerical investigation of the magnetohydrodynamic hybrid nanofluid flow over a stretching surface with mixed

convection: A case of strong suction," *Adv. Mech. Eng.*, vol. 15, no. 6, 2023. https://doi.org/10.1177/16878132231179616.

[17] N. S. Wahid, N. M. Arifin, N. S. Khashi'ie, and I. Pop, "Mixed convection MHD hybrid nanofluid over a shrinking permeable inclined plate with thermal radiation effect," *Alexandria Engineering Journal, vol. 66, pp. 769-783, 2023.* https://doi.org/10.1016/j.aej.2022.10.075

[18] A. E. N. S. Mahdy, T. H. Al-Arabi, A. M. Rashad, and W. Saad, "MHD mixed convective heat transfer of Cu-Al2O3 water hybrid nanofluid over a stretching wedge with ohmic heating," *International Journal of Heat and Technology*, vol. 40, no. 2, pp. 475-481, 2022. 10.18280/ijht.400215

[19] M. Ferdows, B. Alshuraiaan, and N. I. Nima, "Effects of non-Darcy mixed convection over a horizontal cone with different convective boundary conditions incorporating gyrotactic microorganisms on dispersion," *Sci. Rep.*, vol. 12, no. 1, p. 16581, 2022. https://doi.org/10.1038/s41598-022-18549-2

[20] M. Sarfraz, M. Yasir, and M. Khan, "Multiple solutions for non-linear radiative mixed convective hybrid nanofluid flow over an exponentially shrinking surface," *Sci. Rep.*, vol. 13, no. 1, p. 3443, 2023.https://doi.org/10.1038/s41598-023-29892-3